Hindawi
International Journal of Photoenergy
Volume 2021, Article ID 7691202, 12 pages
https://doi.org/10.1155/2021/7691202

Research Article

Electrophoretic Codeposition of MoO_x/MoS_2 Thin Film for Platinum-Free Counter Electrode in Quantum Dot Solar Cells

Thanh Tung Nguyen,[1] Huy Phap Ngo,[2,3] Van Thang Le,[2,4] Le Thanh Nguyen Huynh,[2,3] Viet Hai Le,[2,3] Thai Hoang Nguyen,[2,3] and Hoang Long Ngo[1]

[1]*NTT Hi-Tech Institute, Nguyen Tat Thanh University, 300A Nguyen Tat Thanh, District 4, 700000 Ho Chi Minh City, Vietnam*
[2]*Vietnam National University, Linh Trung Ward, Thu Duc City, 700000 Ho Chi Minh Chi City, Vietnam*
[3]*University of Science, 227 Nguyen Van Cu, District 5, 700000 Ho Chi Minh City, Vietnam*
[4]*Faculty of Materials Technology, Bach Khoa University, 268 Ly Thuong Kiet, District 10, 700000 Ho Chi Minh City, Vietnam*

Correspondence should be addressed to Thai Hoang Nguyen; nthoang@hcmus.edu.vn and Hoang Long Ngo; longnh@ntt.edu.vn

Received 1 August 2021; Revised 30 September 2021; Accepted 18 October 2021; Published 9 November 2021

Academic Editor: Yuanzuo Li

The MoO_x/MoS_2 thin films were manufactured on conducting glass (FTO) from the ethanolic mixture of colloidal molybdenum disulfide (MoS_2) and molybdenum oxides (MoO_x) by electrophoretic deposition method and were used for counter electrode of quantum dot solar cells. Different ramp-rate conditions for electrophoretic deposition as well as bias potential were investigated in an attempt to get the highest possible electrocatalytic activity of polysulfide (S^{2-}/S_n^{2-}) redox couple. In this research, interestingly, by simply using CdS/CdSe/ZnS photoanode and polysulfide electrolyte under 1000 $W.m^{-2}$ AM 1.5 G illumination, the power conversion efficiency of MoO_x/MoS_2-counter-electrode-based QDSC was achieved up to 2.01%, which was double compared to platinum-based counter electrode of QDSCs.

1. Introduction

Nowadays, quantum dot-sensitized solar cells (QDSCs) have emerged as a promising candidate. The construction of QDSCs is derived from dye-sensitized solar cells (DSCs), but using quantum dots (QDs) to replace organic dye molecules as the light harvesting material [1]. Compared to silicon solar cells or DSCs, QDSCs possess the largely improved absorption coefficient (for example, depending on the particle size and the excitation wavelength, those values of CdSe and ZnSe are 10^5–10^6 and $1.8 \times 10^5\ M^{-1}.cm^{-1}$, respectively [2, 3]) and the enhanced photoexcitation. They are also highly light-, thermal-, and moisture-stable, easy to fabricate, and available at low cost [4]; thus, they have been widely studied for harvesting a wide range of light and converting it to electrical energy. Moreover, the small size of QDs can guarantee an excellent film-forming capability [5, 6].

In order to enhance the performance of QDSCs, enormous available literatures commonly focused on improving the three parts of anode, cathode, and the electrolyte. To maximize the durability of QDSCs, polysulfide (S^{2-}/S_n^{2-}) [7, 8] and cobalt complex (Co^{2+}/Co^{3+}) [9, 10] redox couples have been investigated as active electrolytes to replace the iodide/triiodide (I^-/I_3^-) electrolytes that usually cause photocorrosion [7, 8]. In terms of cathodic materials, so far, replacing noble platinum (Pt) has been the main objective of most studies, as Pt might be a superior cathode, but on its low abundance, corrosion by an electrolyte and high cost would prevent industrialization and commercialization [11–13]. To overcome this problem, many attempts have been made in a search for suitable nanomaterial-based cathodes for QDSCs containing polysulfide or cobalt complex redox couples [7, 8, 10]. Compared to Pt, using some kinds of metallic sulfide to prepare the cathode has many advantages, such as low cost, low charge transfer resistance, and good catalytic activity towards polysulfide, etc. [14, 15]. Among them, CuS and CoS have been widely utilized as cathodes in QDSCs [16, 17], each of them as their own advantages and

disadvantages. More specifically, CuS cathodes generally exhibit high values of open circuit potential (V_{oc}) but show low electrocatalytic activity and stability due to sulfur corrosion and poor adhesion to the FTO substrate. On the contrary, CoS-based cathodes have displayed some of the highest fill factor (FF) and power conversion efficiency (η) in QDSCs to date, thanks to their outstanding electrocatalytic activity; yet, they possess relatively low open circuit voltages [18]. As a result, more intensive studies and researches should be conducted in order to develop better and more efficient cathodes. There has also been many attempts to exploit different types of metal sulfides, namely, PbS [14, 15, 19], NiS [20, 21], ZnS [21], FeS_2 [21], and Cu_2S [22], or the combination of different metal sulfides [23–25], which all have the potential to replace expensive Pt with low-cost Pt-free catalysts for cathodes, leading to a promising route to enhancing the power conversion efficiency and reducing the fabrication cost of QDSCs.

For the synthesis of transition metal chalcogenides, numerous approaches have been investigated, such as solvothermal synthesis [26, 27], hydrothermal method [28, 29], in situ deposition methods [30], chemical vapor deposition [31], and many other methods [32, 33]. Among various preparation methods, electrophoretic deposition (EPD), the translation of colloidal charged particles moving to an appropriately biased electrode when applying an electric field across the two electrodes [34], appears to be a straightforward, facile, and low-cost process. Compared to other methods (e.g., coatings, ceramic formation, and chemical vapor deposition), it has many essential advantages such as significantly shorter processing time, simple equipment requirement and no need of binder, high versatility and easy modification, and cost-effectiveness as well as ideal suitability for the good distribution and high quality of products [35–37]. Therefore, EPD is now becoming a captivating technique for the manufacture of biological materials (for example, proteins, enzymes, and cells), as well as solid inorganic nanoparticles, colloids, and polymers, both academically and industrially, which can be applied in many scientific fields, such as chemistry, biology, biochemistry, biotechnology, materials science, and pharmaceutical. Subsequently, various new applications for EPD in the development of both bulk materials and coatings are being reported [37–39], with increasing interest on the utilization of its advantages on nanomaterials [35, 40, 41], biological materials [42, 43], and even solar cells (SCs) [44, 45].

Group 6 transition metal dichalcogenides, such as MoS_2, are promising candidates for photocatalysis and photoelectrochemical applications, in the form of either bulk materials or monolayer thin films, as the photoexcited electrons in MoS_2 can be transferred to the electrode while the holes are removed by the electrolyte, resulting in photocurrent generation [46]. However, up to now, there have been several studies on EPD of MoS_2 thin films for electrocatalytic hydrogen evolution [47, 48], but no attempt on its utilization in manufacturing the cathode for quantum dot solar cells [49]. Therefore, in this work, we present the fabrication of MoO_x/MoS_2 thin films via electrophoresis, their electrochemical characterization, and their catalytic activity as cathodes in QDSC assembly with FTO/TiO_2 photoanode and polysulfide electrolyte.

2. Experimental

2.1. Materials and Reagents. Conducting glass (FTO—2.2 mm thickness, 8 Ω) and TiO_2 paste (DSL 18HR-T) were purchased from Dyesol (Australia). Cadmium nitrate tetrahydrate ($Cd(NO_3)_2.4H_2O$), $(NH_4)_6Mo_7O_{24}.4H_2O$ and thiourea were obtained from Acros Organics (USA). Methanol (CH_3OH), ethanol (C_2H_5OH), potassium chloride (KCl), selenium (Se), and sodium hydroxide (NaOH) were purchased from Merck (Germany), and sodium sulfite andydrous (Na_2SO_3), sulfur (S), and zinc acetate dihydrate ($Zn(CH_3COO)_2.2H_2O$) were from China.

2.2. Synthesis of MoO_x/MoS_2 Thin Films via Electrophoresis

2.2.1. Synthesis of MoO_x/MoS_2 Colloidal Solution. In a typical reaction, ammonium heptamolybdate tetrahydrate, $(NH_4)_6Mo_7O_{24}.4H_2O$, and thiourea, CSN_2H_4, were immersed in a solution of ethanol. The reaction mixture was rapidly heated and kept upon microwave-assisted condition for different time and power. When a great amount of black precipitate occurred, the reaction mixture was cooled down and diluted with ethanol. The solid product was separated by centrifugation, washed several times with absolute ethanol, and then dispersed in ethanol. The characterizations of MoO_x/MoS_2 colloidal solution were detailed in the Supporting Information.

2.2.2. Pretreatment of FTO Glass. FTO glasses (1.2 × 2.5 × 0.22 cm) were washed with distilled water and ethanol twice and then were immersed in 0.1 M HCl/ethanol under ultrasonication. Finally, they were dried at 100°C, cooled down, and were coated with 5 mm perforated tape.

2.2.3. Electrophoresis. Electrophoresis process was conducted using Electrophoresis crosspower equipment (Atto, Japan), Autolab PGSTAT302N and Booster 20 A (Eco Chemie, Netherlands), and Solar Simulator OrielSol1A (Newport, USA). Typically, a pair of treated FTO glasses were parallelly put in a cell containing MoO_x/MoS_2 colloidal solution in ethanol, and the distance between two FTO glasses was 2.5 cm (Figure S3). The MoO_x/MoS_2 colloid was ultrasonicated within 2 hours before electrophoresis to have good dispersion. The fabrication of MoO_x/MoS_2 thin films was conducted under various conditions of (i) electrophoresis potential of 15, 20, 25, and 30 V and (ii) electrophoresis time of 5, 10, 15, 20, and 25 minutes. After the electrophoretic process, the obtained MoO_x/MoS_2 cathodes were calcinated at 350°C for 120 minutes.

2.3. QDSC Assembly. The pristine FTO/TiO_2 photoanodes were prepared following our lab-made process using screen printing method [15]. The SILAR (successive ionic layer adsorption and reaction) method was employed for the preparation of FTO/TiO_2/CdS/CdSe/ZnS electrode, which involved the immersing of the FTO/TiO_2 substrate in a cationic precursor solution (M^{2+}) and then an anionic

Table 1: Cathodic peak current density-j_{pc} ($A.m^{-2}$) and peak potential E_{pc} (vs. Ag/AgCl) of MoS_2 thin films and Pt electrode measured in polysulfide solution containing 5.00 mM sulfur, 20.0 mM Na_2S, and 0.100 M KCl at scan rate of 10 $mV.s^{-1}$.

		t (min)				
		5	10	15	20	25
U (V)	15	*N/A*	0.81 -0.67 V	6.0 -0.74 V	2.0 -0.67 V	*N/A*
	20	13 -0.82 V	**22** -0.72 V	**33** -0.84 V	5.1 -0.67 V	*N/A*
	25	17 -0.82 V	**47** -0.84 V	6.4 -0.74 V	*N/A*	*N/A*
	30	11 -0.74 V	1.5 -0.80 V	12 -0.78 V	*N/A*	*N/A*
Pt electrode (area 0.13 cm^2)				0.21 at -0.57V		

N/A means not available, indicating that there is no detected cathodic peak.

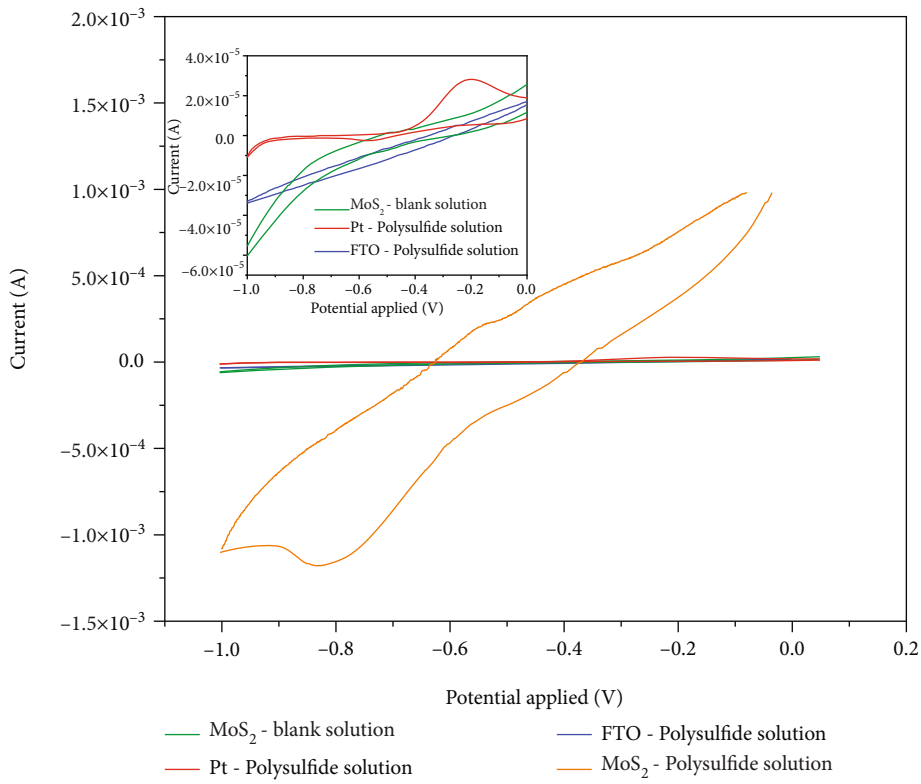

Figure 1: Cyclic voltammograms of MoO_x/MoS_2 thin film (deposited at 25 V in 10 minutes), FTO substrate, and Pt electrode in the blank and the polysulfide solution.

precursor solution (S^{2-} or Se^{2-}), allowing them to react with each other. The complete process is detailed in the Supporting Information (Figure S4).

The FTO/TiO_2/CdS/CdSe/ZnS QDs photoanode and the MoO_x/MoS_2 cathode were sandwiched under heating (150°C). The polysulfide electrolyte, consisted of 0.500 M Na_2S, 0.200 M sulfur, and 0.200 M KCl in the mixture of MeOH/H_2O (3/7, v/v), was injected into the cell, and the holes on the cathode side were sealed using small pieces of Surlyn and microscope cover glass (Figure S5).

2.4. MoO_x/MoS_2 Electrophoretic Thin Film Characterization. The electrochemical properties of MoO_x/MoS_2 thin films on FTO were evaluated via cyclic voltammetry (CV) and electrochemical impedance spectroscopy (EIS) in the three-electrode cell which included Pt as counter electrode and Ag/AgCl as reference electrode. The electrolyte was polysulfide solution containing 5.00 mM sulfur, 20.0 mM Na_2S, and 0.100 M KCl in the solution of MeOH/H_2O (3/7, v/v). A blank solution of 0.100 M KCl was also prepared for the comparison.

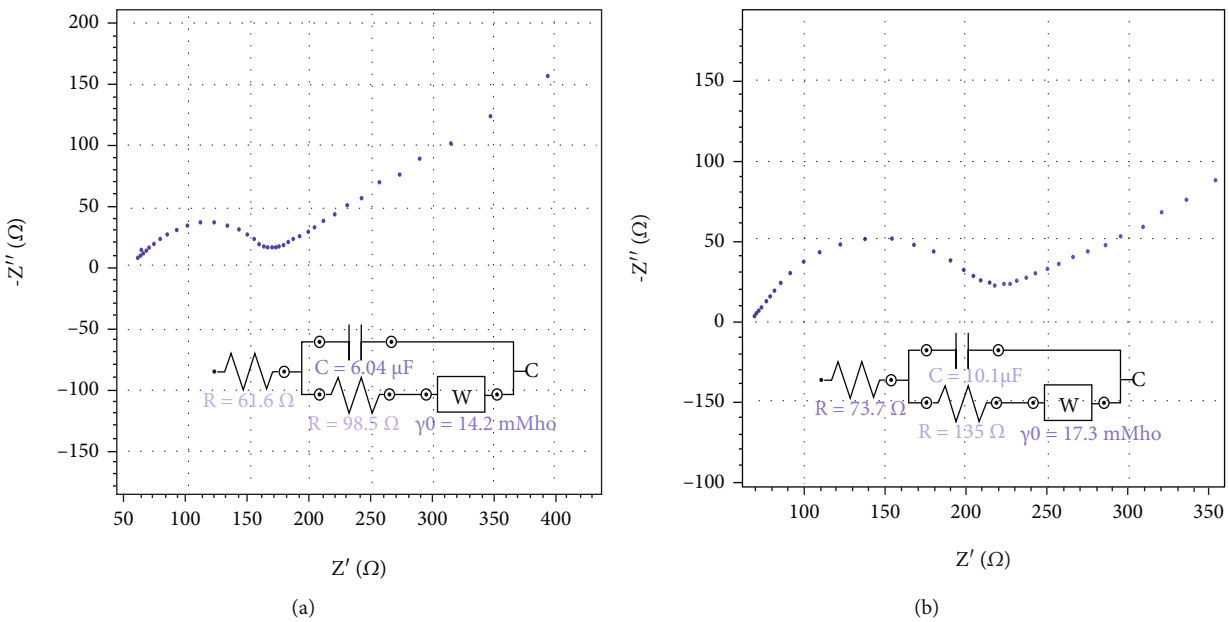

Figure 2: Nyquist plots of MoS_2 deposited at 20 V in (a) 20 minutes and (b) 25 min.

Table 2: Charge transfer resistance R_{ct} (Ω) of MoS_2 thin films and Pt electrode prepared at different time and voltage.

		t (min)				
		5	10	15	20	25
U (V)	15	37.1	50.2	52.6	72.1	77.0
	20	42.5	65.6	95.7	98.5	135
	25	55.6	69.5	105	138	142
	30	57.1	72.3	110	140	309
Pt electrode (area 0.13 cm^2)				307		

The crystalline structures of MoO_x/MoS_2 materials were characterized by X-ray diffraction (XRD) using an X-ray diffractometer D2 Phaser (Bruker, Germany) with a copper anode ($\lambda = 1.54$ Å), and the XRD patterns were acquired in the 2θ range of 10°–80° (0.02° per second). Raman spectroscopy measurements were performed on a LabRAM HR 800 Raman Spectrometer (HORIBA Jobin Yvon) using the green line of an argon-ion laser ($\lambda = 514$ nm) as the excitation source, and the Raman spectra were collected in the wavelength region ranging from 200 to 3000 cm^{-1} at room temperature. The morphology and chemical composition of the thin films were analyzed by scanning electron microscope (SEM) method with a Philips XL 30 FEG SEM (Japan).

3. Results and Discussion

3.1. Electrochemical Properties of MoO_x/MoS_2 Thin Films. Electrocatalytic activity of MoO_x/MoS_2 thin films and Pt electrode was evaluated by cyclic voltammetry (CV), and the characteristic parameters from cyclic voltammogram are detailed in Table 1. Figure 1 shows that the prepared thin films had no electrocatalytic activity in the blank solution, and FTO substrate was incapable of catalyzing

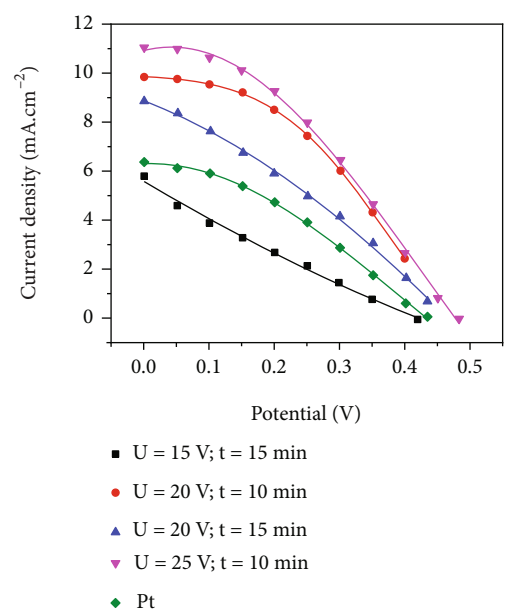

Figure 3: I-V behavior of QDSCs consisting of Pt (area 0.13 cm^2) and MoS_2 thin film electrode (area 0.25 cm^2).

Table 3: Electrochemical parameters of QDSCs using MoS_2 thin film and Pt cathode.

Cathode		J_{sc} (mA.cm^{-2})	V_{oc} (V)	Fill factor	η (%)
Pt		6.41	0.42	0.36	0.984
MoS_2 (15 V; 15 min)	1st	3.54	0.46	0.30	0.492
	2nd	5.84	0.43	0.22	0.549
	3rd	4.57	0.41	0.28	0.536
MoS_2 (15 V; 25 min)	1st	0.522	0.23	0.13	0.0156
	2nd	0.680	0.25	0.15	0.0251
	3rd	0.689	0.25	0.15	0.0252
MoS_2 (20 V; 10 min)	1st	9.86	0.47	0.40	1.87
	2nd	10.1	0.48	0.38	1.85
	3rd	10.3	0.47	0.36	1.74
MoS_2 (20 V; 15 min)	1st	8.90	0.46	0.32	1.29
	2nd	8.50	0.47	0.30	1.21
	3rd	8.60	0.44	0.28	1.04
MoS_2 (25 V; 10 min)	1st	11.1	0.48	0.38	2.01
	2nd	10.9	0.47	0.37	1.90
	3rd	10.6	0.48	0.39	1.97
MoS_2 (30 V; 15 min)	1st	0.818	0.25	0.19	0.0386
	2nd	0.814	0.26	0.19	0.0399
	3rd	0.835	0.26	0.19	0.0404

the desulfurization reaction. Thus, it can be concluded that the change of current intensity in other cyclic voltammograms was caused by the catalysis of MoO_x/MoS_2 thin films for the desulfurization reaction of the polysulfide solution. Additionally, Pt electrode was less active towards polysulfide solution, so at the same measuring conditions, the current density of the Pt electrode was almost significantly lower than that of the MoO_x/MoS_2 thin films, as mentioned in the previous researches. Moreover, according to prior studies, the electrocatalytic activity of MoS_2 in the thin film was positively influenced by the appearance of molybdenum oxides (MoO_x), as a layer of substoichiometric molybdenum oxide (MoO_x, $2 < x < 3$) and other n-type transition metal oxides (TMOs) can be used as a Hole Extraction Layer (HEL) to improve the performance of the QDSCs [50]. MoO_3, which was normally an insulator, was transformed into the oxygen-deficient species of MoO_x and MoO_2 due to surface passivation via the bonding between FTO silicon and TMO oxygen when the thickness was sufficient [51–53]. This MoO_x passivation layer could behave like a barrier for the interfacial recombination, thus could improve the photoelectrochemical performance of the thin films. As a result, molybdenum oxides such as α-MoO_3 were proved to have a good and stable performance in polysulphide electrolyte due to their low charge transfer resistance at the counter electrode–electrolyte interface [54].

The cyclic voltammograms were used to determine the stability of the MoO_x/MoS_2 thin films (Figures S6 and S7 in the Supporting Information), where the spent film can be proved to be stable if the current shows no significant deterioration after 30 cycles of sweep. The current intensity of the 1st cycle and the 30th cycle was not much different. It tended to increase until the 12th cycle and then later gradually decreases. This could be explained that at first, the rate of diffusion of sulfur to the electrode surface was faster than the transfer of charge across the electrode boundary and the electrolyte solution. When a certain value was reached, the diffusion rate decreased and the sulfur concentration on the surface decreases strongly, so the current intensity decreased. At the 30th cycle, the current density was nearly 70% of value of the first cycle. Thus, it was possible to conclude that the MoO_x/MoS_2 thin film had good stability.

Moreover, the charge transfer resistance (R_{ct}) of MoO_x/MoS_2 thin films was measured by electrochemical impedance, which is shown in Figure 2. Charge transfer resistance R_{ct} was the resistance against the process of electron transfer from one phase (MoS_2 electrode) to another (polysulfide solution).

From Table 2, it can be seen that under the same preparation parameters, the resistance of the MoO_x/MoS_2 thin films increased when either increasing the voltage or the electrophoresis time. When the resistance was sufficiently high (greater than 110 Ω), the activity of the thin films decreased dramatically, as shown in Table 1. To achieve optimal electrocatalytic activity, the thin film must be of an appropriate thickness, as resistance is inversely proportional to thickness. If the film is too thick, it will have a high resistance, preventing electrons from moving efficiently from the FTO substrate to the polysulfide solution, lowering the ion conductivity. Electrophoretic deposition allows for easy modification of the film thickness; the higher the voltage applied and the longer the electrophoresis time, the thicker the film becomes [38]. Moreover, from Table 2, the charge

Table 4: Photovoltaic parameters of QDSCs using different types of cathode.

Cathode	Anode	Polysulfide solution	J_{sc} (mA.cm^{-2})	V_{oc} (V)	Fill factor	η_{max} (%)	Reference
FTO/PbS (Cyclic Voltammetry)	TiO_2/CdS/CdSe	0.5 M sulfur, 2.0 M Na_2S, and 0.2 M KCl in the solution of MeOH/H_2O (3/7, v/v)	10.3	0.50	0.45	2.31	Le, V. N. [15]
PbS (Dipping)	FTO/TiO_2/CdS/CdSe	0.1 M sulfur, 1 M Na_2S, and 0.1 M NaOH in H_2O	9.28	0.554	0.588	3.01	Tachan, Z. [14]
FTO/TiO_2/ZnS/Cu_2S (Solvothermal)	TiO_2/CdS/CdSe	0.1 M sulfur, 1 M Na_2S, and 0.1 M NaOH in H_2O	7.13	0.51	0.48	1.83	Giménez, S. [24]
RGO-Cu_2S (spin coating)	FTO/TiO_2/CdS/CdSe/ZnS	1 M sulfur and 1 M Na_2S in H_2O	18.4	0.52	0.48	4.40	Radich, J. G. [22]
FTO/CuS (potentiodynamic electrodeposition)	FTO/TiO_2/CdS-ZnS/CdSe/ZnS	1 M sulfur and 1 M Na_2S in H_2O	13.9	0.55	0.35	2.70	Balis, N. [58]
FTO/CoS (potentiodynamic electrodeposition)	FTO/TiO_2/CdS-ZnS/CdSe/ZnS	1 M sulfur and 1 M Na_2S in H_2O	11.2	0.52	0.32	1.90	Balis, N. [58]
FTO/TiO_2/CuS/CoS (Chemical bath deposition)	FTO/TiO_2/CdS/CdSe/ZnS	0.5 M sulfur, 2.0 M Na_2S, and 0.2 M KCl in the solution of MeOH/H_2O (7:3, v/v)	17.11	N/A	0.554	4.10	Yang, Z. [25]
FTO/NiS (Chemical bath deposition)	FTO/TiO_2/CdS/CdSe/ZnS	2 M sulfur, 1 M Na_2S, and 0.2 M KCl in the solution of MeOH/H_2O (7:3, v/v)	10.38	0.508	0.55	2.97	Kim, H.-J. [20]
FTO/MoO_x/MoS_2 (Electrophoretic Deposition)	FTO/TiO_2/CdS/CdSe/ZnS	5.00 mM sulfur, 20.0 mM Na_2S and 0.100 M KCl in the solution of of MeOH/H_2O (3/7, v/v)	11.1	0.48	0.38	2.01	This work
Pt	FTO/TiO_2/CdS/CdSe/ZnS	5.00 mM sulfur, 20.0 mM Na_2S and 0.100 M KCl in the solution of of MeOH/H_2O (3/7, v/v)	6.41	0.42	0.36	0.984	This work

transfer resistance of most MoO_x/MoS_2 thin films was much smaller compared to Pt electrode (approximately 20 times smaller), leading to the enhancement of electroactivity as measured in Table 1.

Due to the high electroactivity and stability of MoO_x/MoS_2 thin films, they can be used as a counter electrode for quantum dot solar cells, and the performance parameters of which, such as the I–V characteristics, are shown in Figure 3. The short circuit current density J_{sc}, open circuit voltage V_{oc}, fill factor, and power conversion efficiency η of the thin films are summarized in Table 3. All of the MoS_2 cathodes have the open circuit voltage of around 0.4–0.5 V, except for the ones deposited at 15 V/25 min and 30 V/15 min, whose open circuit voltages dropped to around 0.25 V. The decrease observed in both the short circuit current density and the open circuit voltage of these two thin films also leads to poor values of overall power conversion efficiency.

Several factors contribute to the efficiency of QDSC power conversion, including charge carrier recombination with the redox couple at the semiconductor interface, slower hole transfer, and counter electrode performance [55]. Our previous effort to design PbS-QDSC has already resulted in an improvement in the fill factor of the QD [15]. However, due to slower hole transfer to sulfide redox couple, the charge recombination may become the prime limiting factor in achieving higher efficiency of QDSC [56]. Hence, the mid-gap states created by the doping of semiconductor films such as MoS_2 can cause electrons to get trapped and protect them from charge recombination with holes and/or oxidized polysulfide electrolyte [57]. As a result, numerous studies are being conducted to better understand the charge transfer dynamics and recombination processes in systems.

The maximum efficiency of QDSCs using MoS_2 thin film (deposited at 25 V in 10 minutes) is 2.01%, which was nearly twice as high when compared to QDSCs with a Pt cathode (0.984%). Its higher fill factor also suggests that the sum of the charge-transfer resistance at the counter electrode–electrolyte interface and the series resistance for the MoS_2 thin film is lower than for the Pt cathode, which is evidently associated with the higher catalytic activity towards the charge transfer reaction at the counter electrode–polysulfide electrolyte interface, as proved by the cyclic voltammetry (Figure 1) and EIS measurements (Table 2). This result is also consistent with the results of electrochemical activity that we measured in Table 1.

Table 4 compares the electrochemical parameters of QDSCs based on different types of metal chalcogenide cathode materials, as they not only exhibit excellent electrocatalytic activity towards the polysulfide electrolyte but also possess good physical and chemical stability, low cost, and ease of fabrication. The MoO_x/MoS_2 cathode exhibited satisfactory performance specifications compared to other types of sulfide counter electrodes constructed using different methods.

3.2. Characterization of MoO_x/MoS_2 Thin Film. In order to understand the good electrochemical properties and satisfactory QDSC application, the MoO_x/MoS_2 thin film was characterized. To begin with, nanostructure mixture of molybdenum disulfide and molybdenum oxide (MoO_x/MoS_2) has been synthesized by a facile and rapid method of microwave, and the diameter of the particles in the colloidal solution was measured by laser particle size analyzer LA-960A, which is shown in Figure S1 and Table S1. In this strategy, microwave irradiation accelerates the synthesis of MoS_2 to several minutes owing to the special localized heating via dipolar polarization and ionic conduction, allowing higher heating rates and shorter processing time [59], with the potential to increase the amount of uniformly smaller nuclei which enables the formation of the final product in smaller diameter [60].

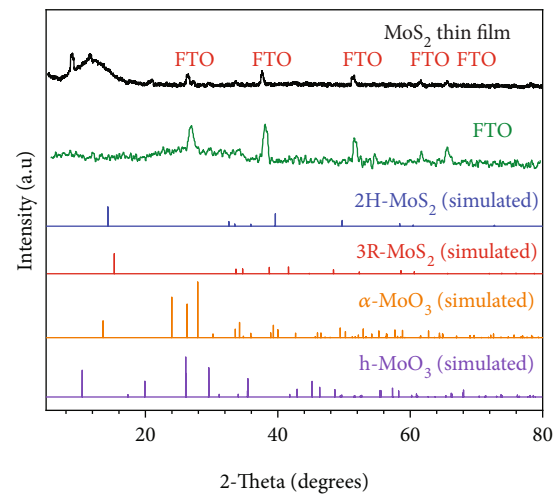

Figure 4: XRD pattern of MoO_x/MoS_2 thin film deposited at 25 V in 10 minutes on FTO glass using ethanol solvent.

The structure and morphology of MoS_2 were characterized by X-ray diffraction (XRD), Raman spectroscopy (Raman), and scanning electron microscopy (SEM). Firstly, MoS_2 powder after electrophoresis from MoS_2 colloidal solution was analyzed by XRD (Figure S2). The elemental analysis of the obtained powder indicates that the products seem to be a mixture of molybdenum sulfides and molybdenum oxides (Table S2). Since thiourea may act as a reducing agent, there might also be some undesired reduction by-products, as Afanasiev et al. showed that the reduction of aqueous ammonium heptamolybdate at different reaction conditions might yield different compounds such as binary sulfides of $MoS_{5.6}$, MoS_6, and MoS_3 as well as binary oxides of MoO_3 and MoO_2 [61]; still there was no peak to be observed in the XRD diagram. There was no peak appearing to match with the peak positions of the crystalline phases of MoS_2, especially the absence of the reflections at $2\theta = 14.5^\circ$ or 37.4°, which suggests a large extent of destacking in the synthesized MoS_2 [62, 63]. The products exhibited their poor crystallinity and were almost amorphous. The experimental results suggest that the structure of the synthesized samples using microwave heating was randomly oriented, with crystal defects or strains owing to the curvature of the layers. The broad peaks at the low diffraction angle of less than 20° (which is commonly found in nanomaterials)

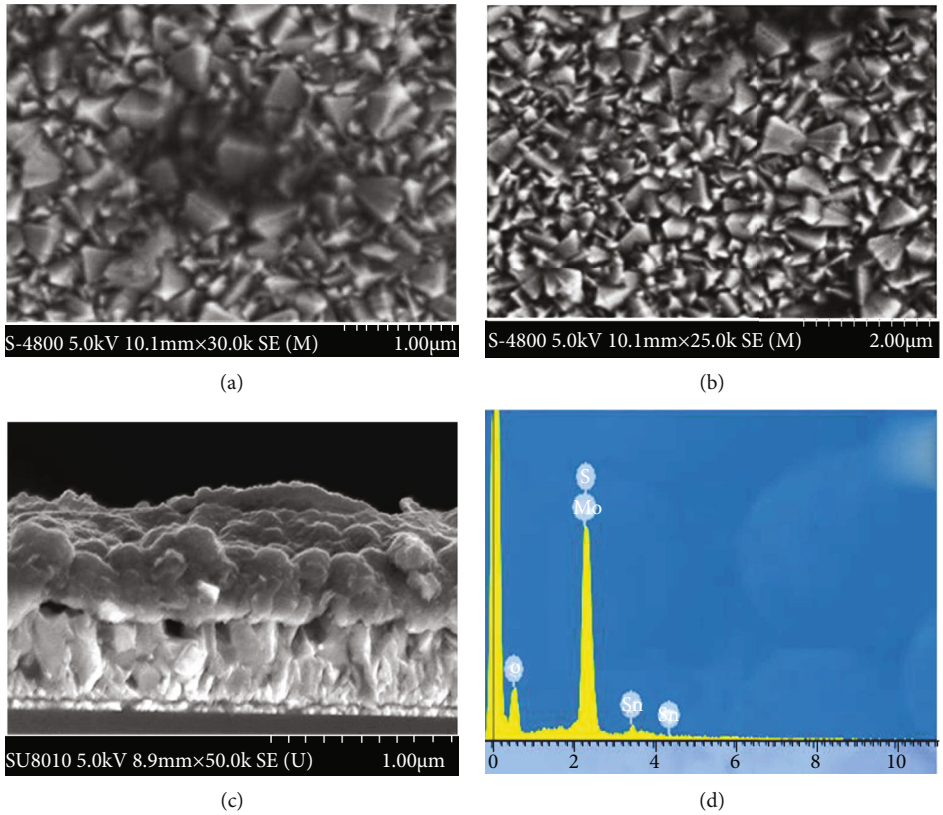

Figure 5: FE-SEM images and EDS spectrum of MoO_x/MoS_2 thin film ($U = 25$ V, $t = 10$ minutes) deposited on FTO glass at various magnifications: (a) 2.0 μm, (b) 1.0 μm, (c) cross section, and (d) EDS spectrum.

have not been determined, but they also confirm the a highly disordered and poorly crystalline structure of the MoS_2 materials [64, 65]. It is considered a satisfying result, as a study of Miki et al. concluded that amorphous MoS_2 is better than other crystalline phases when used as a cathode in lithium batteries because of its much greater conductivity and significant life cycle of lithium batteries [66].

Subsequently, the thin films after electrophoresis from MoO_x/MoS_2 colloidal solution were also analyzed by XRD, and the result is shown in Figure 4. Similar to the XRD spectrum of MoS_2, MoS_2 films were believed to be amorphous. These results were also consistent with the results of XRD analysis for MoS_2 colloidal solution [67]. The molybdenum oxide appeared to be a mixture of MoO_2 and MoO_3. As observed in the XRD spectrum, besides the peaks of FTO, there are some other peaks which may belong to MoO_2 as the reduction–decomposition product of the heptamolybdate salt [68] and MoO_3 as the calcination products at 350°C [69, 70]. More specifically, the peaks at $2\theta = 9.0$, 17.5, 21.1, and 29.5° belong to the hexagonal h-MoO_3 (ICSD #75417) [71], and other peaks at $2\theta = 11.6$, 27.3, and 33.6° belong to orthorhombic α-MoO_3 (ICSD #35076) [72]. The diffraction peaks of MoO_2 at $2\theta = 25.9$, 37.0, 53.6, 60.6, and 67.6° [73] may be overlapped or may be too small to be observed in the XRD diagram. Based on TGA results of Kovács et al., $(NH_4)_6Mo_7O_{24}.4H_2O$ will release H_2O and NH_3 to form $(NH_4)_8Mo_{10}O_{34}$ in the first decomposition step (from 25 to 180°C), then $(NH_4)_2Mo_4O_{13}$ in the second decomposition step (from 180 to 270°C), and finally MoO_3 in the third decomposition step (from 270 to 370°C), with the increasing amount of α-MoO_3 and decreasing amount of h-MoO_3 when the temperature is elevated [74].

Next, the surface morphology and composition of MoO_x/MoS_2 thin film deposited at 25 V in 10 minutes were analyzed by field emission scanning electron microscope with Oxford Energy-dispersive X-ray Spectrometer (FE-SEM/EDS). Figure 5 shows that the surface of the thin film covered with MoO_x and MoS_2 was relatively uniform and was a little bit rough. It is possible that the surface defects were formed during the calcination process, as thin layer of molybdenum oxides appeared quickly during high temperature oxidation of the defective MoS_2 layer and then vaporized leaving the flaws on the material surface [75, 76]. Nevertheless, these defects contribute as good catalytic sites for desulfurization reaction. Additionally, from the SEM images, MoS_2 particle size was estimated about 200–300 nm. By EDS analysis (Figure 5(d) and Table S2), besides the Sn and O peaks of the FTO glass, Mo and S were present as major elements of the thin film. Together with the FE-SEM/EDS results, the Raman spectrum in Figure 6 also exhibited the vibration of Mo-O and Mo-S bonds of MoO_x/MoS_2 thin film, as well as the Sn-O bond of the FTO glass [77, 78]. There was also Sn-S bond due to the sulfidation of the FTO glass (SnO) at high temperature. These interactions help make the thin films become more adhesive to FTO substrate; thus, electrons can easily move

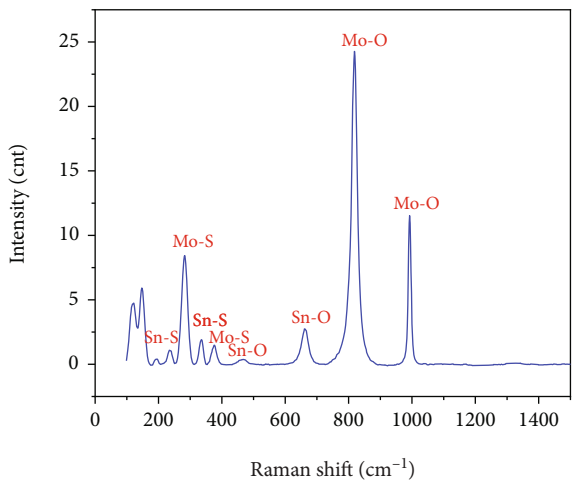

Figure 6: Raman spectra of MoO_x/MoS_2 thin film deposited at 25 V for 10 minutes on FTO glass.

from the substrate to the surface of the thin film to react with sulfur in the polysulfide solution.

4. Conclusion

MoO_x/MoS_2 thin films have successfully been fabricated via electrophoresis method with good catalytic activity towards polysulfide solution after thermal treatment process. The thin films contain molybdenum sulfide and different molybdenum oxides and possess high stability, uniformity, and adhesiveness on FTO substrate. The film thickness could be modified by electrophoretic deposition with different value of applied voltage and the electrophoresis time. Moreover, the charge transfer resistance on the boundary between the MoO_x/MoS_2 thin films and polysulfide solution is also much lower than the Pt electrode. The best condition for the electrophoresis of MoS_2 colloid dispersed in ethanol solvent was also established to achieve the best electrocatalytic activity towards polysulfide solution, which is at 25 V in 10 minutes. QDSC assembly testing showed that the best cell fabricated with a FTO/TiO_2(3)/CdS(3)/CdSe(5)/ZnS(2) anode and a MoO_x/MoS_2 cathode deposited at 25 V in 10 minutes yielded the highest efficiency of 2.01% with $J_{sc} = 11.1\,mA/cm^2$, $V_{oc} = 0.48\,V$, FF = 0.38, and an active area of $0.25\,cm^2$ under AM 1.5 illumination. This result was nearly double compared to Pt cathode in the polysulfide electrolyte, suggesting that MoS_2 thin films are capable of replacing Pt as a cathode in QDSCs. Furthermore, electrophoretic deposition method was shown to be an effective pathway to fabricate thin film, thanks to its simple equipment requirements, short processing time, and the ability to control the thickness and the distribution of the product. Future researches on this matter will focus on various preparation parameters, such as molybdenum precursors, reducing agents, or calcination temperature, in order to achieve different ratio of MoO_x/MoS_2 or MoO_2/MoO_3, therefore leading to better enhancement in the activity of the cathodes.

Data Availability

The research data used to support the findings of this study are included within the article.

Conflicts of Interest

The authors declare that there is no conflict of interest.

Supplementary Materials

Figure S1: scheme of particle size distribution. Figure S2: XRD pattern of MoS_2. Figure S3: electrophoretic preparation of MoO_x/MoS_2 electrode on FTO. Figure S4: process of preparation of electrode FTO/TiO_2/CdS/CdSe/ZnS by the SILAR method. Figure S5: schematic of the fabricated device. Figure S6: cyclic voltammograms of MoS_2 ($U = 25\,V$, $t = 10$ minutes, and area $0.25\,cm^2$) after 30 scanning cycles. Figure S7: cyclic voltammograms of MoS_2 ($U = 20\,V$, $t =$ 20 minutes, and area $0.25\,cm^2$) after 30 scanning cycles. Table S1: diameter of the MoO_x/MoS_2 particles. Table S2: the elemental composition analysis of MoS_2 powder. *(Supplementary Materials)*

References

[1] G. Hodes, "Comparison of dye- and semiconductor-sensitized porous nanocrystalline liquid junction solar cells," *The Journal of Physical Chemistry C*, vol. 112, no. 46, pp. 17778–17787, 2008.

[2] W. C. W. Chan, D. J. Maxwell, X. Gao, R. E. Bailey, M. Han, and S. Nie, "Luminescent quantum dots for multiplexed biological detection and imaging," *Current Opinion in Biotechnology*, vol. 13, no. 1, pp. 40–46, 2002.

[3] D. Dorfs, A. Salant, I. Popov, and U. Banin, "ZnSe quantum dots within CdS nanorods: a seeded-growth type-II system," *Small*, vol. 4, no. 9, pp. 1319–1323, 2008.

[4] Z. Pan, H. Rao, I. Mora-Sero, J. Bisquert, and X. Zhong, "Quantum dot-sensitized solar cells," *Chemical Society Reviews*, vol. 47, no. 20, pp. 7659–7702, 2018.

[5] Z. Ding, Z. Hao, B. Meng, Z. Xie, J. Liu, and L. Dai, "Few-layered graphene quantum dots as efficient hole-extraction layer for high- performance polymer solar cells," *Nano Energy*, vol. 15, pp. 186–192, 2015.

[6] H. B. Yang, Y. Q. Dong, X. Wang, S. Y. Khoo, and B. Liu, "Cesium carbonate functionalized graphene quantum dots as stable electron-selective layer for improvement of inverted polymer solar cells," *ACS Applied Materials & Interfaces*, vol. 6, no. 2, pp. 1092–1099, 2014.

[7] Y.-L. Lee and C.-H. Chang, "Efficient polysulfide electrolyte for CdS quantum dot-sensitized solar cells," *Journal of Power Sources*, vol. 185, no. 1, pp. 584–588, 2008.

[8] Y. Tachibana, H. Y. Akiyama, Y. Ohtsuka, T. Torimoto, and S. Kuwabata, "CdS quantum dots sensitized TiO_2 sandwich type photoelectrochemical solar cells," *Chemistry Letters*, vol. 36, no. 1, pp. 88-89, 2007.

[9] H. J. Lee, J.-H. Yum, H. C. Leventis et al., "CdSe quantum dot-sensitized solar cells exceeding efficiency 1% at full-sun intensity," *The Journal of Physical Chemistry C*, vol. 112, no. 30, pp. 11600–11608, 2008.

[10] H. Lee, M. Wang, P. Chen et al., "Efficient CdSe quantum dot-sensitized solar cells prepared by an improved successive ionic layer adsorption and reaction process," *Nano Letters*, vol. 9, no. 12, pp. 4221–4227, 2009.

[11] T. Battumur, S. H. Mujawar, Q. T. Truong et al., "Graphene/carbon nanotubes composites as a counter electrode for dye-sensitized solar cells," *Current Applied Physics*, vol. 12, pp. e49–e53, 2012.

[12] S. Yun, Y. Liu, T. Zhang, and S. Ahmad, "Recent advances in alternative counter electrode materials for Co-mediated dye-sensitized solar cells," *Nanoscale*, vol. 7, no. 28, pp. 11877–11893, 2015.

[13] S. Yun, P. D. Lund, and A. Hinsch, "Stability assessment of alternative platinum free counter electrodes for dye-sensitized solar cells," *Energy & Environmental Science*, vol. 8, no. 12, pp. 3495–3514, 2015.

[14] Z. Tachan, M. Shalom, I. Hod, S. Rühle, S. Tirosh, and A. Zaban, "PbS as a highly catalytic counter electrode for polysulfide-based quantum dot solar cells," *The Journal of Physical Chemistry C*, vol. 115, no. 13, pp. 6162–6166, 2011.

[15] V. N. Le, T. H. Nguyen, V. H. Le, and T. P. T. Nguyen, "Lead sulfide cathode for quantum dot solar cells: electrosynthesis and characterization," *Journal of Electronic Materials*, vol. 46, no. 1, pp. 274–281, 2016.

[16] W. Ke, G. Fang, H. Lei et al., "An efficient and transparent copper sulfide nanosheet film counter electrode for bifacial quantum dot-sensitized solar cells," *Journal of Power Sources*, vol. 248, pp. 809–815, 2014.

[17] K. Meng, P. K. Surolia, O. Byrne, and K. R. Thampi, "Efficient CdS quantum dot sensitized solar cells made using novel Cu2S counter electrode," *Journal of Power Sources*, vol. 248, pp. 218–223, 2014.

[18] H. Yuan, J. Lu, X. Xu et al., "Electrochemically deposited CoS films as counter electrodes for efficient quantum dot-sensitized solar cells," *Journal of the Electrochemical Society*, vol. 160, no. 9, pp. H624–H629, 2013.

[19] A. D. Mani, M. Deepa, P. Ghosal, and C. Subrahmanyam, "Novel single pot synthesis of metal (Pb, Cu, Co) sulfide nanomaterials -towards a quest for paintable electrode materials that supersedes Pt electrode," *Electrochimica Acta*, vol. 139, pp. 365–373, 2014.

[20] H.-J. Kim, D.-J. Kim, S. S. Rao et al., "Highly efficient solution processed nanorice structured NiS counter electrode for quantum dot sensitized solar cells," *Electrochimica Acta*, vol. 127, pp. 427–432, 2014.

[21] Q. Han, H. Zheng, and M. Wu, "Designing Metal-Sulfide-Sphere Counter-Electrode Catalysts for ZnO-Nanorod-Array-Based Quantum-Dot-Sensitized Solar Cells," *European Journal of Inorganic Chemistry*, vol. 2017, no. 32, pp. 3787–3793, 2017.

[22] J. G. Radich, R. Dwyer, and P. V. Kamat, "Cu_2S reduced graphene oxide composite for high-efficiency quantum dot solar cells. Overcoming the redox limitations of S^{2-}/S_n^{2-} at the counter electrode," *Journal of Physical Chemistry Letters*, vol. 2, no. 19, pp. 2453–2460, 2011.

[23] L. Givalou, M. Antoniadou, D. Perganti et al., "Electrodeposited cobalt-copper sulfide counter electrodes for highly efficient quantum dot sensitized solar cells," *Electrochimica Acta*, vol. 210, pp. 630–638, 2016.

[24] S. Gimenez, I. Mora-Sero, L. Macor et al., "Improving the performance of colloidal quantum-dot-sensitized solar cells," *Nanotechnology*, vol. 20, no. 29, p. 295204, 2009.

[25] Z. Yang, C.-Y. Chen, C.-W. Liu, C.-L. Li, and H.-T. Chang, "Quantum dot-sensitized solar cells featuring CuS/CoS electrodes provide 4.1% efficiency," *Advanced Energy Materials*, vol. 1, no. 2, pp. 259–264, 2011.

[26] J. Gao, Q. Li, H. Zhao et al., "One-pot synthesis of uniform Cu_2O and CuS hollow spheres and their optical limiting properties," *Chemistry of Materials*, vol. 20, no. 19, pp. 6263–6269, 2008.

[27] Y. Hu, Z. Zheng, H. Jia, Y. Tang, and L. Zhang, "Selective synthesis of FeS and FeS_2 nanosheet films on iron substrates as novel photocathodes for tandem dye-sensitized solar cells," *The Journal of Physical Chemistry C*, vol. 112, no. 33, pp. 13037–13042, 2008.

[28] S. S. Kalanur, S. Y. Chae, and O. S. Joo, "Transparent Cu1. 8S and CuS thin films on FTO as efficient counter electrode for quantum dot solar cells," *Electrochimica Acta*, vol. 103, pp. 91–95, 2013.

[29] W. Dong, X. Wang, B. Li et al., "Hydrothermal synthesis and structure evolution of hierarchical cobalt sulfide nanostructures," *Dalton Transactions*, vol. 40, no. 1, pp. 243–248, 2011.

[30] J. Xu, J. Xiao, J. Dong, Y. Luo, D. Li, and Q. Meng, "A new in-situ preparation method to CuS electrodes for CdS/CdSe co-sensitized solar cells," *Electrochimica Acta*, vol. 127, pp. 180–185, 2014.

[31] G. Du, W. Li, and Y. Liu, "Filling carbon nanotubes with Co_9S_8 nanowires through in situ catalyst transition and extrusion," *The Journal of Physical Chemistry C*, vol. 112, no. 6, pp. 1890–1895, 2008.

[32] Y. Yin, C. K. Erdonmez, A. Cabot, S. Hughes, and A. P. Alivisatos, "Colloidal synthesis of hollow cobalt sulfide nanocrystals," *Advanced Functional Materials*, vol. 16, no. 11, pp. 1389–1399, 2006.

[33] Q. Wang, L. Jiao, H. Du et al., "Novel flower-like CoS hierarchitectures: one-pot synthesis and electrochemical properties," *Journal of Materials Chemistry*, vol. 21, no. 2, pp. 327–329, 2011.

[34] O. O. Van der Biest and L. J. Vandeperre, "Electrophoretic deposition of materials," *Annual Review of Materials Science*, vol. 29, no. 1, pp. 327–352, 1999.

[35] J. H. Dickerson and A. R. Boccaccini, *Electrophoretic Deposition of Nanomaterials*, New York, Springer, 2012.

[36] M. Wang, L. D. Duong, J. S. Oh et al., "Large-area, conductive and flexible reduced graphene oxide (RGO) membrane fabricated by electrophoretic deposition (EPD)," *ACS applied materials & interfaces*, vol. 6, no. 3, pp. 1747–1753, 2014.

[37] P. Sarkar, D. De, T. Uchikochi, and L. Besra, "Electrophoretic deposition (EPD): fundamentals and novel applications in fabrication of advanced ceramic microstructures," *InElectrophoretic Deposition of Nanomaterials*, pp. 181–215, 2012.

[38] L. Besra and M. Liu, "A review on fundamentals and applications of electrophoretic deposition (EPD)," *Progress in Materials Science*, vol. 52, no. 1, pp. 1–61, 2007.

[39] P. Amrollahi, J. S. Krasinski, R. Vaidyanathan, L. Tayebi, and D. Vashaee, "Electrophoretic deposition (EPD): Fundamentals and applications from nano-to micro-scale structures," in *Handbook of Nanoelectrochemistry*, Springer International Publishing, Switzerland, 2015.

[40] I. Corni, M. P. Ryan, and A. R. Boccaccini, "Electrophoretic deposition: from traditional ceramics to nanotechnology," *Journal of the European Ceramic Society*, vol. 28, no. 7, pp. 1353–1367, 2008.

[41] A. P. Terzyk, M. Zięba, S. Koter et al., "Recent Developments in the Electrophoretic Deposition of Carbon Nanomaterials," *In Porous Materials*, pp. 113–137, 2021.

[42] M. Ammam and J. Fransaer, "AC-electrophoretic deposition of metalloenzymes: catalase as a case study for the sensitive and selective detection of H2O2," *Sensors and Actuators B: Chemical*, vol. 160, no. 1, pp. 1063–1069, 2011.

[43] B. Neirinck, L. Van Mellaert, J. Fransaer, O. Van der Biest, J. Anné, and J. Vleugels, "Electrophoretic deposition of bacterial cells," *Electrochemistry Communications*, vol. 11, no. 9, pp. 1842–1845, 2009.

[44] M. Hamadanian, A. Gravand, and V. Jabbari, "High performance dye-sensitized solar cells (DSSCs) achieved via electrophoretic technique by optimizing of photoelectrode properties," *Materials Science in Semiconductor Processing*, vol. 16, no. 5, pp. 1352–1359, 2013.

[45] M. Marandi, N. Torabi, and F. Ahangarani Farahani, "Facile fabrication of well-performing CdS/CdSe quantum dot sensitized solar cells through a fast and effective formation of the CdSe nanocrystalline layer," *Solar Energy*, vol. 207, pp. 32–39, 2020.

[46] L. A. King, W. Zhao, M. Chhowalla, D. J. Riley, and G. Eda, "Photoelectrochemical properties of chemically exfoliated MoS_2," *Journal of Materials Chemistry A*, vol. 1, no. 31, 2013.

[47] J. Dong, X. Zhang, J. Huang et al., "Boosting heterojunction interaction in electrochemical construction of MoS2 quantum dots@TiO2 nanotube arrays for highly effective photoelectrochemical performance and electrocatalytic hydrogen evolution," *Electrochemistry Communications*, vol. 93, pp. 152–157, 2018.

[48] A. Bayat, M. Zirak, and E. Saievar-Iranizad, "Vertically aligned MoS_2 quantum dots/nanoflakes heterostructure: facile deposition with excellent performance toward hydrogen evolution reaction," *ACS Sustainable Chemistry & Engineering*, vol. 6, no. 7, pp. 8374–8382, 2018.

[49] T. Sogabe, Q. Shen, and K. Yamaguchi, "Recent progress on quantum dot solar cells: a review," *Journal of Photonics for Energy*, vol. 6, no. 4, 2016.

[50] J. Gao, C. L. Perkins, J. M. Luther et al., "n-type transition metal oxide as a hole extraction layer in PbS quantum dot solar cells," *Nano Letters*, vol. 11, no. 8, pp. 3263–3266, 2011.

[51] L. G. Gerling, C. Voz, R. Alcubilla, and J. Puigdollers, "Origin of passivation in hole-selective transition metal oxides for crystalline silicon heterojunction solar cells," *Journal of Materials Research*, vol. 32, no. 2, pp. 260–268, 2016.

[52] L. G. Gerling, S. Mahato, A. Morales-Vilches et al., "Transition metal oxides as hole-selective contacts in silicon heterojunctions solar cells," *Solar Energy Materials and Solar Cells*, vol. 145, pp. 109–115, 2016.

[53] H. Nasser, F. Es, M. Zolfaghari Borra et al., "On the application of hole-selective MoO_x as full-area rear contact for industrial scale p-type c-Si solar cells," *Progress in Photovoltaics: Research and Applications*, vol. 29, no. 3, pp. 281–293, 2020.

[54] P. S. Tamboli, M. R. Prasad, V. S. Kadam, R. S. Vhatkar, H. M. Pathan, and S. S. Mahajan, "α-MoO3-C composite as counter electrode for quantum dot sensitized solar cells," *Solar Energy Materials and Solar Cells*, vol. 161, pp. 96–101, 2017.

[55] P. V. Kamat, K. Tvrdy, D. R. Baker, and J. G. Radich, "Beyond photovoltaics: semiconductor nanoarchitectures for liquid-junction solar cells," *Chemical Reviews*, vol. 110, no. 11, pp. 6664–6688, 2010.

[56] V. Chakrapani, D. Baker, and P. V. Kamat, "Understanding the role of the sulfide redox couple (S^{2-}/S_n^{2-}) in quantum dot-sensitized solar cells," *Journal of the American Chemical Society*, vol. 133, no. 24, pp. 9607–9615, 2011.

[57] P. K. Santra and P. V. Kamat, "Mn-doped quantum dot sensitized solar cells: a strategy to boost efficiency over 5%," *Journal of the American Chemical Society*, vol. 134, no. 5, pp. 2508–2511, 2012.

[58] N. Balis, V. Dracopoulos, K. Bourikas, and P. Lianos, "Quantum dot sensitized solar cells based on an optimized combination of ZnS, CdS and CdSe with CoS and CuS counter electrodes," *Electrochimica Acta*, vol. 91, pp. 246–252, 2013.

[59] C. Gabriel, S. Gabriel, E. H. Grant et al., "Dielectric parameters relevant to microwave dielectric heating," *Chemical Society Reviews*, vol. 27, no. 3, 1998.

[60] X. Meng and F. S. Xiao, "Green routes for synthesis of zeolites," *Chemical Reviews*, vol. 114, no. 2, pp. 1521–1543, 2014.

[61] P. Afanasiev, G.-F. Xia, G. Berhault, B. Jouguet, and M. Lacroix, "Surfactant-assisted synthesis of highly dispersed molybdenum sulfide," *Chemistry of Materials*, vol. 11, no. 11, pp. 3216–3219, 1999.

[62] Z. Matusinovic, R. Shukla, E. Manias, C. G. Hogshead, and C. A. Wilkie, "Polystyrene/molybdenum disulfide and poly(methyl methacrylate)/molybdenum disulfide nanocomposites with enhanced thermal stability," *Polymer Degradation and Stability*, vol. 97, no. 12, pp. 2481–2486, 2012.

[63] X. Wang, Y. P. Zhang, and Z. Q. Chen, "Morphological evolution of MoS_2 nanosheets by chemical vapor deposition," *Chalcogenide Letters*, vol. 13, no. 8, pp. 351–357, 2016.

[64] I. Bezverkhy, P. Afanasiev, and M. Lacroix, "Aqueous preparation of highly dispersed molybdenum sulfide," *Inorganic Chemistry*, vol. 39, no. 24, pp. 5416-5417, 2000.

[65] Y. Tian, X. Zhao, L. Shen et al., "Synthesis of amorphous MoS2 nanospheres by hydrothermal reaction," *Materials Letters*, vol. 60, no. 4, pp. 527–529, 2006.

[66] Y. Miki, D. Nakazato, H. Ikuta, T. Uchida, and M. Wakihara, "Amorphous MoS_2 as the cathode of lithium secondary batteries," *Journal of Power Sources*, vol. 54, no. 2, pp. 508–510, 1995.

[67] T. M. N. Nguyen, "Microwave–assisted synthesis of molybdenum disulfide (MoS2)," *Vietnam Journal of Science and Technology*, vol. 55, no. 1B, 2018.

[68] K. Chen, X.-M. Zhang, X.-F. Yang et al., "Electronic structure of heterojunction MoO2/g-C3N4 catalyst for oxidative desulfurization," *Applied Catalysis B: Environmental*, vol. 238, pp. 263–273, 2018.

[69] G. Mitran, F. Neatu, O. D. Pavel, M. M. Trandafir, and M. Florea, "Behavior of molybdenum–vanadium mixed oxides in selective oxidation and disproportionation of toluene," *Materials (Basel)*, vol. 12, no. 5, 2019.

[70] H. Hu, C. Deng, J. Xu, K. Zhang, and M. Sun, "Metastable h-MoO_3 and stable α-MoO_3 microstructures: controllable synthesis, growth mechanism and their enhanced photocatalytic activity," *Journal of Experimental Nanoscience*, vol. 10, no. 17, pp. 1336–1346, 2015.

[71] G. T. Santos, A. A. Felix, and M. O. Orlandi, "Ultrafast growth of h-MoO3 microrods and its acetone sensing performance," *Surfaces*, vol. 4, no. 1, pp. 9–16, 2020.

[72] X. Chan, N. Akter, P. Yang et al., "Fundamental study of furfuryl alcohol dehydration reaction over molybdenum oxide catalyst," *Molecular Catalysis*, vol. 466, pp. 19–25, 2019.

[73] J. Besnardiere, C. Surcin, V. Buissette et al., "Nonclassical crystallization and size control of ultra-small MoO_2 nanoparticles in water," *Particle & Particle Systems Characterization*, vol. 32, no. 2, pp. 251–257, 2015.

[74] T. N. Kovács, D. Hunyadi, A. L. A. de Lucena, and I. M. Szilágyi, "Thermal decomposition of ammonium molybdates," *Journal of Thermal Analysis and Calorimetry*, vol. 124, no. 2, pp. 1013–1021, 2016.

[75] W. L. Spychalski, M. Pisarek, and R. Szoszkiewicz, "Microscale insight into oxidation of single MoS_2 crystals in air," *The Journal of Physical Chemistry C*, vol. 121, no. 46, pp. 26027–26033, 2017.

[76] J. A. Kropp, A. Sharma, W. Zhu, C. Ataca, and T. Gougousi, "Surface defect engineering of MoS_2 for atomic layer deposition of TiO_2 films," *ACS Applied Materials & Interfaces*, vol. 12, no. 42, pp. 48150–48160, 2020.

[77] H. Li, Q. Zhang, C. C. R. Yap et al., "From bulk to monolayer MoS_2: evolution of Raman scattering," *Advanced Functional Materials*, vol. 22, no. 7, pp. 1385–1390, 2012.

[78] B. C. Windom, W. G. Sawyer, and D. W. Hahn, "A Raman spectroscopic study of MoS_2 and MoO_3: applications to tribological systems," *Tribology Letters*, vol. 42, no. 3, pp. 301–310, 2011.